applied sciences

MDPI

Article

Resonant Coupling Effects in a Double-Layer THz Bandpass Filter

Tao Gao, Feng Huang *, Yanqing Chen, Weilin Zhu, Xuewei Ju and Xiangfeng Wang *

School of Mechanical Engineering and Automation, Fuzhou University, Fuzhou 350108, China; gaotfzu@163.com (T.G.); yqchen@fzu.edu.cn (Y.C.); weilin_zhu123@163.com (W.Z.); xueweiju1991@gmail.com (X.J.)

* Correspondence: huangf@fzu.edu.cn (F.H.); xfwang@fzu.edu.cn (X.W.); Tel.: +86-591-22866262

Received: 19 June 2020; Accepted: 15 July 2020; Published: 22 July 2020

Featured Application: THz bandpass filter design.

Abstract: Cascading similar frequency selective surfaces (FSSs) improves the roll-off rate and frequency selectivity of THz bandpass filters. However, resonant coupling between FSS layers causes anomalous transmission peaks. In this work, we have employed an equivalent circuit model to analyze a double-layer FSS structure with periodic cross apertures at different interlayer spacing. We found that the anomalous peaks can be attributed to the resonant coupling between the upper and lower layer FSSs, and their periodic appearance with changing interlayer spacing is related to the half-wavelength repeatability of the circuit. We have fabricated a double-layer FSS sample using femtosecond laser micromachining and measured it using time-domain THz spectroscopy. The results using the equivalent circuit model agree with the Finite-Difference Time-Domain (FDTD) and experimental results.

Keywords: bandpass filters; equivalent circuit model; FSS; time-domain THz spectroscopy

1. Introduction

Terahertz (THz) waves generally refer to electromagnetic radiation in the 0.1–10 THz frequency range. THz waves have potential applications in bio-sensing, satellite communication, military radar, object imaging, environmental monitoring, and medical diagnosis [1]. Studies on THz functional devices such as waveguides, polarizers, modulators, antennas, switches, and bandpass filters are particularly important for applications of THz technology [2–13]. THz bandpass filters are one of the key components to effectively control and manipulate THz waves. THz filters can be grouped into the following types: photonic crystal filters [7,8], filters based on metamaterials [10–13], and frequency selective surfaces (FSSs) [14–16].

FSS-based filters are composed of periodically arranged apertures on a metal foil. They are easy to fabricate and have a controllable central frequency and a low insertion loss. Most of the commercially available THz bandpass filters are FSS-based. Compared with single-layer FSSs, double-layer FSSs have the characteristics of better frequency selectivity, a higher roll-off rate, and a lower angle sensitivity, suitable for narrowband and multiband operations [17–19]. However, periodically appearing anomalous transmission peaks will appear in double-layer stacking when the interlayer spacing and wavelength are of the same order of magnitude [19,20]. What causes these anomalous transmission peaks and their periodic appearance with spacing is important not only in filter design but also for fundamental understanding. Usually, the analysis of this kind of structure relies on the use of commercial full-wave electromagnetic solvers such as the Finite-Difference Time-Domain (FDTD) method. However, it is difficult to understand the physical mechanisms behind the computed

transmission spectra of stacked FSS structures. Equivalent circuit models (ECMs) have been utilized to analyze anomalous transmission peaks and show a good agreement with commercial full-wave electromagnetic solvers in the microwave region [21–25].

In this work, we presented a method based on an ECM to examine the THz anomalous transmission phenomena of a double-layer cross FSS structure, and analyzed the evolution and origin of these transmission peaks at different interlayer spacing. We fabricated a double-layer FSS sample using femtosecond laser micromachining and measured it using time-domain THz spectroscopy. The results obtained by the ECM agree with the FDTD and experimental results.

2. Theory and Experiments

The double-layer FSS structure consists of periodically arranged cross apertures perforated on 10 μm Al foils as shown in Figure 1a. Two FSS layers are stacked parallel with no dielectric substrate in between and without lateral shift. Structural parameters of the cross unit include arm length l, arm width w, thickness t, period p, and double-layer spacing d.

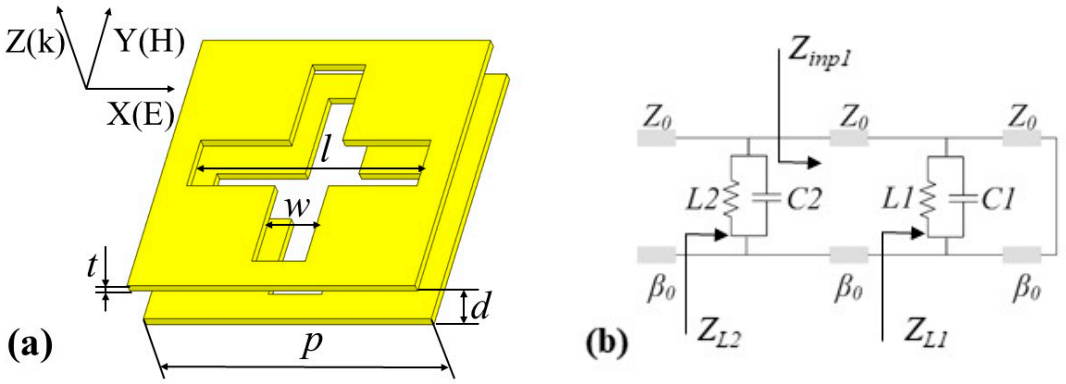

Figure 1. (**a**) Schematics of the double-layer cross frequency selective surface (FSS) unit structure. l, w, t, p, and d represent the arm length, arm width, thickness, period, and spacing of the double-layer FSS structure, respectively; (**b**) equivalent circuit model of the double FSS structure.

The equivalent inductance L and capacitance C are different for FSSs with different shapes and structural parameters. For some commonly used FSS elements, such as rectangles, holes, squares, crosses, etc., the values of L and C can be calculated using theoretical formulas [26–28]. However, the accuracy of L and C values obtained using formulas is low, and the error is magnified further after multi-layer stacking. Therefore, we used an inversion method, which employs FDTD (FDTD Solutions, Lumerical Inc., Vancouver, BC, Canada) to calculate the equivalent L and C of the single-layer FSS, in order to concentrate on the coupling effects of the multi-layer stacking. In the FDTD simulation, we used periodic boundary conditions for X and Y directions, and perfect matching layers along the Z direction. The material is Al with a plasma frequency of 2.24×10^{16} rad/s, and a damping coefficient of 1.12×10^{14} rad/s. The polarization of the terahertz waves is along the X direction.

Firstly, the transmission coefficient and reflection coefficient of the single-layer FSS were calculated by FDTD. Because the single-layer FSS is a reciprocal symmetric network, we have $S_{12} = S_{21}$ (transmission coefficient), $S_{11} = S_{22}$ (reflection coefficient). In this way, all the elements in the S matrix of the single-layer FSS can be obtained. Then, the impedance matrix of single-layer FSS was calculated by Equation (1) according to the conversion relationship of the parameters for a two-port network [29,30]:

$$Z_{FSS} = Z_0 \frac{(1+S_{11})(1-S_{22}) + S_{12}S_{21}}{(1-S_{11})(1-S_{22}) - S_{12}S_{21}} \quad (1)$$

where Z_0 is the characteristic impedance of free space. For a slot structure, it is equivalent to the inductance L and capacitance C connected in parallel. The admittance can be expressed as

$$Y_{FSS} = \frac{1}{Z_{FSS}} = \mathrm{j}2\pi fC + \frac{1}{\mathrm{j}2\pi fL} \tag{2}$$

Assuming that the values of inductance L and capacitance C are stable within the frequency range, by selecting two frequency points f_a and f_b in the sub-wavelength region ($\lambda > p$) and using Equation (2), the equivalent parameters L and C of the circuit can be calculated as follows:

$$L = \frac{(f_b/f_a - f_a/f_b)}{j2\pi[f_b Y_{FSS}(f_a) - f_a Y_{FSS}(f_b)]} \tag{3}$$

$$C = \frac{(Y_{FSS}(f_a)/f_b - Y_{FSS}(f_b)/f_a)}{j2\pi(f_a/f_b - f_b/f_a)} \tag{4}$$

By cascading the LC oscillation circuits corresponding to the upper and lower layers, we obtained the ECM of the double-layer FSS as shown in Figure 1b. One can see that at Z_{inp1} port, the electromagnetic wave passes through only one FSS layer and the interlay air. At Z_{L2} port, the electromagnetic wave has passed through two FSS layers, and Z_{L2} contains the coupling effect between the two FSS layers. Z_{L1}, Z_{inp1}, and Z_{L2} in the ECM can be expressed as

$$Z_{L1} = \frac{Z_0 \times Z_{FSS}}{Z_0 + Z_{FSS}} \tag{5}$$

$$Z_{inp1} = Z_0 \frac{Z_{L1} + jZ_0 tan(\beta_0 \times d)}{Z_0 + jZ_{L1} tan(\beta_0 \times d)} \tag{6}$$

$$Z_{L2} = \frac{Z_{inp1} \times Z_{FSS}}{Z_{inp1} + Z_{FSS}} \tag{7}$$

where $\beta_0 = \omega/c$, ω is the angular frequency and c is the speed of light in a vacuum. Z_{L2} obtained from Equation (7) is the load impedance of ECM. The reflection coefficient Γ and the transmittance T of the ECM can be calculated as follows:

$$\Gamma = \frac{Z_{L2} - Z_0}{Z_{L2} + Z_0} \tag{8}$$

$$T = 1 - \Gamma^2 \tag{9}$$

Single-layer FSSs with geometrical parameters l = 280 μm, w = 65 μm, t = 10 μm, and p = 350 μm were fabricated on 10 μm Al foils using a femtosecond laser micromachining system [13,31]. The femtosecond laser has a wavelength of 800 nm, a pulse width of 45 fs, and a repetition rate of 1 KHz. The Al foil was placed on a computer-controlled two-dimensional translation platform with a moving speed of 500 μm/s and an acceleration of 500 μm/s^2, and the laser power used was 10 mW. The calculated focal spot size is 1.44 μm in diameter, and the power density (or irradiance) is about 0.48 MW/cm^2.

We stacked two single-layer FSSs to form a double-layer structure. To precisely assemble the two FSS layers, we first put one layer clinging to the other layer (spacing d = 0). We aligned the cross aperture arrays using visible light projection. Then, we moved one filter mounted on a one-dimensional translation stage with respect to the other fixed filter to control the spacing between the two layers. The sample was measured using a home-made time-domain THz spectroscopy system, which employs a Ti: Sapphire femtosecond amplifier and ZnTe crystals for both THz generation and detection. The system has a usable spectral range from 0.2–2.5 THz and a power spectrum dynamic range >50 dB. Time-domain signals were acquired over a time window of about 25 ps, corresponding to a frequency resolution of 40 GHz ($\Delta f = 1/T_{\mathrm{window}}$).

3. Results and Discussion

Figure 2a,b shows the FDTD (blue), ECM (green), and experimental (red) results when the interlayer spacing d equals 555 and 585 μm, respectively. The ECM results are credible only when the calculated wavelength is larger than the period p = 350 μm [24]. The transition point at $\lambda \approx p$ = 350 μm ($f = c/\lambda \approx$ 0.857 THz) was traditionally referred to as Wood's anomaly [32]. Thus, the simulation THz range is set from 0.1 to 0.85 THz. In the simulated range, the results obtained by ECM agree with those obtained by FDTD and experiments. We see three peaks in each experimental spectrum, which are labeled as f_1, f_2, f_3 for d = 555 μm and f_4, f_5, f_6 for d = 585 μm. The ECM spectrum shows narrower peaks, because both experiments and FDTD simulations have a limited time window. In the time-domain THz spectroscopy measurements, the time window is confined by the internal reflection pulse of a 1 mm ZnTe detection crystal, appearing at about 21.6 ps after the main THz pulse.

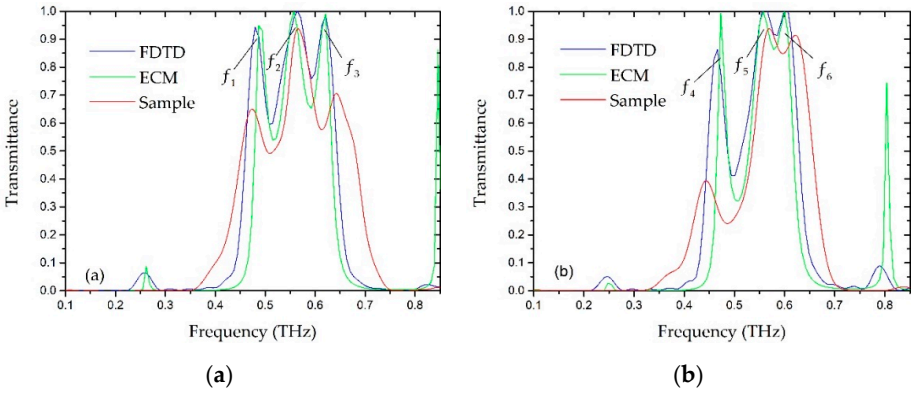

Figure 2. Comparison between the experimental, equivalent circuit model (ECM), and Finite-Difference Time-Domain (FDTD) results for spacing d = 555 μm (**a**) and 585 μm (**b**).

We scanned the interlayer spacing d from 50 to 1050 micron to explore the evolution of the transmission peaks at different interlayer spacing using ECM. We obtained the transmittance contour map for a range from 0.1 to 0.85 THz, as shown in Figure 3a, which coincides with the results of FDTD simulation (Figure 3b). The transmission peak, which does not vary with the spacing d, is highlighted with a white line B, and two transmission lines, periodically appearing like wings on both sides of line B with varying d, are highlighted as line A_i and C_i (i denotes the series of wings).

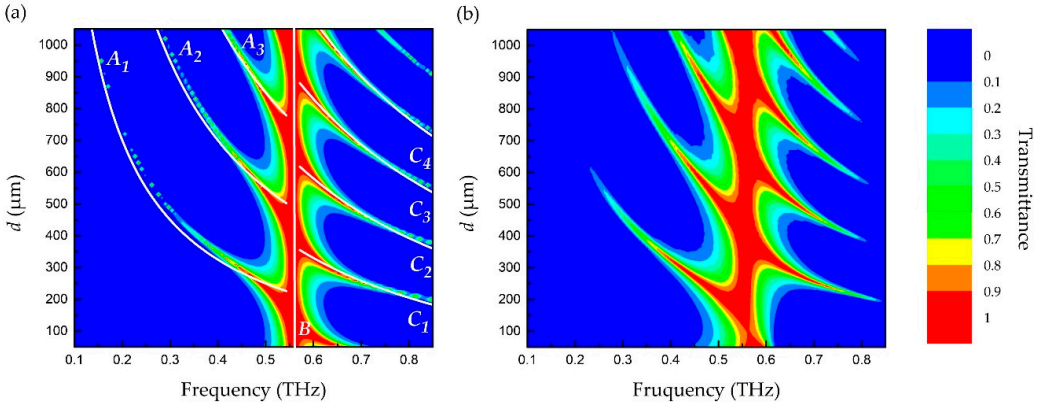

Figure 3. (**a**) The transmittance contour map in a THz range from 0.1 to 0.85 THz for spacing d changing from 50 to 1050 μm, calculated by ECM. Line B highlights the central transmission peak, and line A_i and line C_i highlight the left and right wings, respectively. i denotes the series of wings. (**b**) The transmittance contour map calculated by FDTD.

It can be seen from Figures 2 and 3 that the positions of f_2 and f_5 coincide with that of line B, at about 0.557 THz. Obviously, the peak highlighted by line B is the intrinsic transmission of the single-layer FSS. In order to analyze the effect of double-layer coupling, we need to look into Z_{L2}. Equation (6) shows that Z_{L2} is composed of Z_{inp1} and Z_{FSS} connected in parallel. The air interlayer is represented by Z_0 and β_0. Z_{inp1} represents the impedance of the first layer FSS plus interlayer air, and Z_{FSS} represents the equivalent impedance of the second FSS layer.

The single-layer slot-type FSS is equivalent to the parallel connection of inductance and capacitance. When resonance occurs, the inductance reactance and capacitance reactance of the parallel circuit are equal, that is, the inductance current and the capacitance current are equal. Because the inductance current lags behind the voltage by 90° in phase and the capacitance current leads the voltage by 90° in phase, the phase difference between the inductance current and the capacitance current is exactly 180°. At this time, there is no current passing through the circuit (no loss) and the transmittance of the FSS is the maximum.

Similarly, for the double-layer FSS, the total input impedance Z_{L2} is equivalent to the parallel connection of Z_{inp1} and Z_{FSS}. As we know, the real part of the impedance represents resistance, while the imaginary part represents reactance. A positive imaginary part represents inductance, while a negative imaginary part represents capacitance. When the transmittance is the maximum, the circuit resonates, and the imaginary parts of the paralleled impedance Z_{inp1} and Z_{FSS} should be equal in amplitude but with opposite signs. Therefore, we add up the imaginary parts of Z_{inp1} and Z_{FSS} and plot the sum in Figure 4a for d = 555 μm and d = 585 μm, and Figure 4b is the enlarged view at the sum equal to zero. As it can be seen from the figure, for d = 555 μm, at about 0.487 and 0.621 THz, the sum lines pass zero. At these two zero points, the upper and lower FSSs resonate and the anomalous transmission peaks f_1 and f_3 appear. For d = 585 μm, at 0.473 and 0.607 THz, the sum lines pass zero, corresponding to the anomalous transmission peaks of f_4 and f_6. Therefore, according to ECM theory, the anomalous transmission peaks (f_1, f_3, f_4, and f_6) can be attributed to the resonant coupling between double FSS layers. At 0.564 THz, that is, the transmission peaks f_2 and f_5 (also the position of line B), the sum is not equal to zero, because the peak corresponds to the intrinsic transmission of the single-layer FSS and is irrelevant to the double-layer coupling. In addition, the ECM also predicts peaks at about 0.25 and 0.8 THz, which were not observed in our experimental data. For the peak at 0.25 THz, the real part of Z_{L2} is only about a few ohms, mismatching with the impedance of the free space (377 ohms), indicating a weak resonance/peak. The peak at 0.8 THz is too sharp to be observed in our experiments because we have a limited frequency resolution.

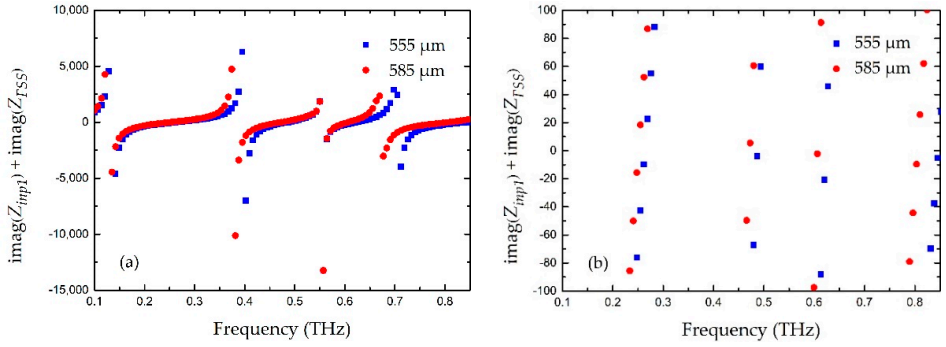

(**a**) (**b**)

Figure 4. (**a**) The sum of the imaginary parts of Z_{inp1} and Z_{FSS}; (**b**) the enlarged view at the sum equal to zero.

Furthermore, for the periodic appearance of the anomalous transmission peaks/wings, we found that Z_{inp1} has a certain periodicity. Increasing d by integer multiple of half wavelength ($\frac{m\lambda}{2}$) and using Equation (6) to calculate Z_{inp1} ($d+\frac{m\lambda}{2}$), we have

$$Z_{inp1}\left(d+\frac{m\lambda}{2}\right)=Z_0\frac{Z_{L1}+jZ_0tan(\beta_0\times d+m\pi)}{Z_0+jZ_{L1}tan(\beta_0\times d+m\pi)}=Z_0\frac{Z_{L1}+jZ_0tan(\beta_0\times d)}{Z_0+jZ_{L1}tan(\beta_0\times d)}=Z_{inp} \quad (10)$$

This indicates that the impedances of two points with $\frac{m\lambda}{2}$ spacing on the transmission line are equal.

We can convert the repetitive phase $\Delta\varphi = m\pi$ (m is a positive integer) into distance. The repetition period of d is calculated as follows:

$$\Delta d = \frac{mc}{2f} \tag{11}$$

By using Equation (11) and substituting different m values, we can plot lines A_i and C_i, which coincide with the center of the periodic wings shown in Figure 3. Therefore, by calculating the sum of the imaginary parts of Z_{inp1} and Z_{FSS}, we can predict these periodically appearing anomalous transmission peaks/wings that are caused by the resonant coupling between the two FSS layers. Our interpretation is consistent with the explanation in terms of a strongly coupled Fabry–Pérot resonator [21].

In addition, if we draw a horizontal line at a larger spacing d in Figure 3, we obtain more anomalous peaks. They can also be perfectly predicted and explained using our model. At THz frequencies, the thicknesses of commercially available substrates are comparable to the free-space wavelength. Substrates cause unwanted substrate resonances or Fabry–Pérot resonances, which otherwise degrade the transmission characteristics of the cascaded FSS structure, smearing out the anomalous transmission features observed in this work.

4. Conclusions

In this work, we have shown that anomalous THz transmission of a double-layer FSS structure can be explained by ECM. The transmission peak not affected by the layer spacing is attributed to the intrinsic transmission of the single-layer FSS, while the side anomalous transmission peaks are due to the resonant coupling between the equivalent capacitive and inductive reactance of the upper and lower layer FSSs. Their periodic appearance with changing spacing d is associated with the half-wavelength repeatability of the circuit. The ECM results agree with the FDTD and experimental results.

Author Contributions: Data curation, W.Z.; Formal analysis, T.G.; Funding acquisition, F.H. and X.W.; Investigation, X.J. and X.W.; Methodology, T.G. and F.H.; Project administration, F.H.; Software, Y.C.; Validation, Y.C., W.Z., and X.J.; Writing—Original draft, T.G.; Writing—Review and editing, X.W. All authors have read and agreed to the published version of the manuscript.

Funding: This research was funded by the Engineering Research Center for CAD/CAM of Fujian Universities (K201708), and in part by the Guiding Projects of Fujian Science and Technology Department (2019H0005).

Conflicts of Interest: The authors declare no conflict of interest.

References

1. Mittleman, D.M. Perspective: Terahertz science and technology. *J. Appl. Phys.* **2017**, *122*, 230901. [CrossRef]
2. Zangeneh-Nejad, F.; Safian, R. A graphene-based THz ring resonator for label-free sensing. *IEEE Sens. J.* **2016**, *16*, 4338–4344. [CrossRef]
3. Zangeneh-Nejad, F.; Safian, R. Hybrid graphene–molybdenum disulphide based ring resonator for label-free sensing. *Opt. Commun.* **2016**, *371*, 9–14. [CrossRef]
4. Rahm, M.; Li, J.S.; Padilla, W.J. Thz wave modulators: A brief review on different modulation techniques. *J. Infrared Millim. Terahertz Waves* **2013**, *34*, 1–27. [CrossRef]
5. Yarahmadi, M.; Moravvej-Farshi, M.K.; Yousefi, L. Subwavelength graphene-based plasmonic THz switches and logic gates. *IEEE Trans. Terahertz Sci. Technol.* **2015**, *5*, 725–731. [CrossRef]
6. Zangeneh-Nejad, F.; Safian, R. Significant enhancement in the efficiency of photoconductive antennas using a hybrid graphene molybdenum disulphide structure. *J. Nanophotonics* **2016**, *10*, 036005. [CrossRef]
7. Zangeneh-Nejad, F.; Fleury, R. Topological analog signal processing. *Nat. Commun.* **2019**, *10*, 2058. [CrossRef]
8. Zhang, H.; Guo, P.; Chen, P.; Chang, S.; Yuan, J. Liquid-crystal-filled photonic crystal for terahertz switch and filter. *J. Opt. Soc. Am. B* **2009**, *26*, 101–106. [CrossRef]
9. He, J.; Liu, P.; He, Y.; Hong, Z. Narrow band-pass tunable terahertz filter based on photonic crystal cavity. *Appl. Opt.* **2012**, *51*, 776–779. [CrossRef]

10. Zhou, X.; Yin, X.; Zhang, T.; Chen, L.; Li, X. Ultrabroad terahertz band-pass filter by hyperbolic metamaterial waveguide. *Opt. Express* **2015**, *23*, 11657–11664. [CrossRef]
11. Hu, F.; Fan, F.; Zhang, X.; Jiang, W.; Chen, Y.; Li, P.; Yin, X.; Zhang, W. Intensity modulation of a terahertz band-pass filter: Utilizing image currents induced on MEMS reconfigurable metamaterials. *Opt. Lett.* **2018**, *43*, 17–20. [CrossRef]
12. Papari, G.P.; Koral, C.; Andreone, A. Geometrical dependence on the onset of surface plasmon polaritons in thz grid metasurfaces. *Sci. Rep.* **2019**, *9*, 924. [CrossRef] [PubMed]
13. Papari, G.P.; Nivas, J.J.J.; Koral, C.; Allahyari, E.; Andreone, A. Engineering of high quality factor THz metasurfaces by femtosecond laser ablation. *Opt. Laser Technol.* **2020**, *128*, 106159. [CrossRef]
14. Gao, B.; Ren, Z.; Lin, Y.; Chen, Y.; Wang, X. Design and verification of an integrated free-Standing thick-screen FSS radome. *IEEE Antennas Wirel. Propag. Lett.* **2018**, *17*, 1630–1634. [CrossRef]
15. Lin, Y.; Yao, H.; Ju, X.; Chen, Y.; Zhong, S.; Wang, X. Free-standing double-layer terahertz band-pass filters fabricated by femtosecond laser micro-machining. *Opt. Express* **2017**, *25*, 25125–25134. [CrossRef] [PubMed]
16. Chen, K.; Li, Z.; Liu, J.; Duan, R.; Wang, Y.; Zhang, W.; Cai, B.; Chen, L.; Zhu, Y. A study of FSS in terahertz range for polarization modulation purpose. *IEEE Photonics Technol. Lett.* **2013**, *25*, 1613–1615. [CrossRef]
17. Vegesna, S.; Zhu, Y.; Bernussi, A.; Saed, M. Terahertz two-layer FSSs with improved transmission characteristics. *IEEE Trans. Terahertz Sci. Technol.* **2012**, *2*, 441–448. [CrossRef]
18. Ebrahimi, A.; Nirantar, S.; Withayachumnankul, W.; Bhaskaran, M. Second-order terahertz bandpass FSS with miniaturized elements. *IEEE Trans. Terahertz Sci. Technol.* **2015**, *5*, 761–768. [CrossRef]
19. Rao, L.; Yang, D.; Zhang, L.; Li, T.; Xia, S. Design and experimental verification of terahertz wideband filter based on double-layered metal hole arrays. *Appl. Opt.* **2012**, *51*, 912–916. [CrossRef]
20. Miyamaru, F.; Hangyo, M. Anomalous terahertz transmission through double-layer metal hole arrays by coupling of surface plasmon polaritons. *Phys. Rev. B* **2005**, *71*, 165408. [CrossRef]
21. Kaipa, C.S.R.; Yakovlev, A.B.; Medina, F.; Mesa, F.; Hibbins, A.P. Circuit modeling of the transmissivity of stacked two-dimensional metallic meshes. *Opt. Express* **2010**, *18*, 13309–13320. [CrossRef] [PubMed]
22. Barzegar-Parizi, S. Analysis of stacked structures composed of arrays of thick slits: An accurate analytical circuit model. *Plasmonics* **2018**, *13*, 1711–1719. [CrossRef]
23. Molero, C.; Rodríguez-Berral, R.; Mesa, F.; Medina, F. Wideband analytical equivalent circuit for coupled asymmetrical nonaligned slit arrays. *Phys. Rev. E* **2017**, *95*, 023303. [CrossRef]
24. Kaipa, C.S.R.; Yakovlev, A.B.; Medina, F.; Mesa, F. Transmission through stacked 2D periodic distributions of square conducting patches. *J. Appl. Phys.* **2012**, *112*, 033101. [CrossRef]
25. Costa, F.; Monorchio, A.; Manara, G. An Overview of Equivalent Circuit Modeling Techniques of Frequency Selective Surfaces and Metasurfaces. *ACES J.* **2014**, *29*, 960–976.
26. Gao, M.; Abadi, S.; Behdad, N. A dual-band, inductively-coupled miniaturized-element FSS with higher-order bandpass response. *IEEE Trans. Antennas Propag.* **2016**, *64*, 3729–3734. [CrossRef]
27. Hokmabadi, M.P.; Wilbert, D.S.; Kung, P.; Kim, S.M. Design and analysis of perfect terahertz metamaterial absorber by a novel dynamic circuit model. *Opt. Express* **2013**, *21*, 16455–16465. [CrossRef]
28. Langley, R.J.; Parker, E.A. Equivalent circuit model for arrays of square loops. *Electron. Lett.* **1982**, *18*, 294–296. [CrossRef]
29. Pozar, D.M. *Microwave Engineering*; John Wiley & Sons: New York, NY, USA, 2011; pp. 189–192.
30. Frickey, D.A. Conversions between S, Z, Y, H, ABCD, and T parameters which are valid for complex source and load impedances. *IEEE Trans. Microw. Theory Tech.* **1994**, *42*, 205–211. [CrossRef]
31. Chen, Y.Q.; Gao, B.P.; Lin, Y.Z.; Ju, X.W.; Wang, J.; Wang, X.F. Metal wire grid THz polarizer fabricated by femtosecond laser micro-machining. *Chin. J. Lasers* **2018**, *45*, 0802005. [CrossRef]
32. Wood, R.W. On a remarkable case of uneven distribution of light in a diffraction grating spectrum. *Philos. Mag.* **1902**, *4*, 269–275. [CrossRef]